electronic materials

Article

Theoretical Prediction of Heterogeneous Integration of Dissimilar Semiconductor with Various Ultra-Thin Oxides and 2D Materials

Md Nazmul Hasan, Chenxi Li, Junyu Lai and Jung-Hun Seo *

Department of Materials Design and Innovation, University at Buffalo, The State University of New York (SUNY), Buffalo, NY 14260, USA; mhasan9@buffalo.edu (M.N.H.); cli73@buffalo.edu (C.L.); jlai5@buffalo.edu (J.L.)

* Correspondence: junghuns@buffalo.edu

Theoretical and mathematical background:

The main, well-established argument of the semiconductor's tunneling mechanism is that the electron is considered a continuous wave function. When a wave function incident at the barrier, part of the wave is transmitted through the barrier, and part of the wave is reflected back. Hence, the transmitted wave is considered as tunneling electrons. Two possible cases could arise that the particle's total energy can either be higher than the potential barrier or lower than the potential barrier. If the particle energy is sufficiently high enough, it can roll over the barrier that meets classical mechanics. But if the particle energy is not sufficiently high enough, then tunneling happens.

To explain this tunneling phenomenon, we have considered the one-dimensional Schrödinger wave equation as follows

$$\left(-\frac{\hbar^2}{2m^*}\Delta^2 + V(x)\right)\Psi(x) = E\Psi(x) \quad (1)$$

Where the m^* is effective mass, $\hbar$ is plank constant, V(x) is barrier height and considered piecewise constant. It will not be straightforward if the V(x) varies with the position in the x-direction. For a thin rectangle potential barrier, the height at the Interface can have three different zones. If "a" is the barrier's thickness, the incident wave would see barrier height, V=0 before and after the transmission, but its height is considered V=Vo in the middle of the barrier. So, in three regions, the Schrödinger wave equation can be written as follows:

$$\left(-\frac{\hbar^2}{2m^*}\Delta^2 + V(x)\right)\Psi_1(x) = E\Psi_1(x), \text{ region 1: [x<0 and V=0]} \quad (2)$$

$$\left(-\frac{\hbar^2}{2m^*}\Delta^2 + V(x)\right)\Psi_2(x) = E\Psi_2(x), \text{ region 2: [x<0<x<a and V=V}_0\text{]} \quad (3)$$

$$\left(-\frac{\hbar^2}{2\mathrm{m}^*}\Delta^2 + \mathrm{V(x)}\right)\Psi_3(\mathrm{x}) = \mathrm{E}\Psi_3(\mathrm{x}), \text{ region 3: [x>a and V=0]} \quad (4)$$

The solutions of equation (2–4) can be assumed as follows:

$$\Psi_1(x) = Ae^{ik_1x} + Be^{-ik_1x} \quad (5)$$

$$\Psi_2(x) = Ce^{ik_2x} + De^{-ik_2x} \quad (6)$$

$$\Psi_3(x) = Ee^{ik_3x} + Fe^{-ik_3x} \quad (7)$$

Where $k_1{}^2 = 2m^*E/\hbar^2$, $k_2{}^2 = 2m^*(E - V_0)/\hbar^2$ and $k_3{}^2 = \frac{2m^*E}{\hbar^2} = k_1{}^2$

Since there is no potential disturbance after the wave is wholly transmitted in the 3rd region, F=0, the probability of finding an electron in region 3 is constant and like to appear. After considering so many boundary conditions and solving equation (5–7), it can be written as follows:

$$\frac{B}{A} = \frac{(k_1^2 - k_2^2)(1 - e^{i2ak_2})}{(k_1 + k_2)^2 - (k_1 + k_2)^2 e^{i2ak_2}} \tag{8}$$

$$\frac{F}{A} = \frac{4k_1k_2(e^{i(k_2-k_1)a})}{(k_1 + k_2)^2 - (k_1 + k_2)^2 e^{i2ak_2}} \tag{9}$$

The tunneling probability is the modulus squared of the transmitted wave ratio to the incident wave function. So it can be defined as:

$$T = \left|\frac{F}{A}\right|^2 = \frac{4E(V_0 - E)}{V_0^2 sinh^2(k_2a) + 4E(V_0 - E)} \tag{10}$$

In the case of a thick barrier, the electron wave will be reflected even the total given energy is greater than the barrier height potential. Hence all-electron can't tunnel through the potential barrier. **Figure S1** shows a schematic illustration of the energy bandgap with an ultra-thin oxide tunneling layer. The conduction band offset (ΔE_C) for different ultrathin oxides with n-GaAs, considered at the tunneling barrier potential for electrons. Similarly, the valence band offset (ΔE_V) for various ultra-thin oxides with p-Si. The electron and hole can easily tunnel thru the oxides if the thickness gets thinner.

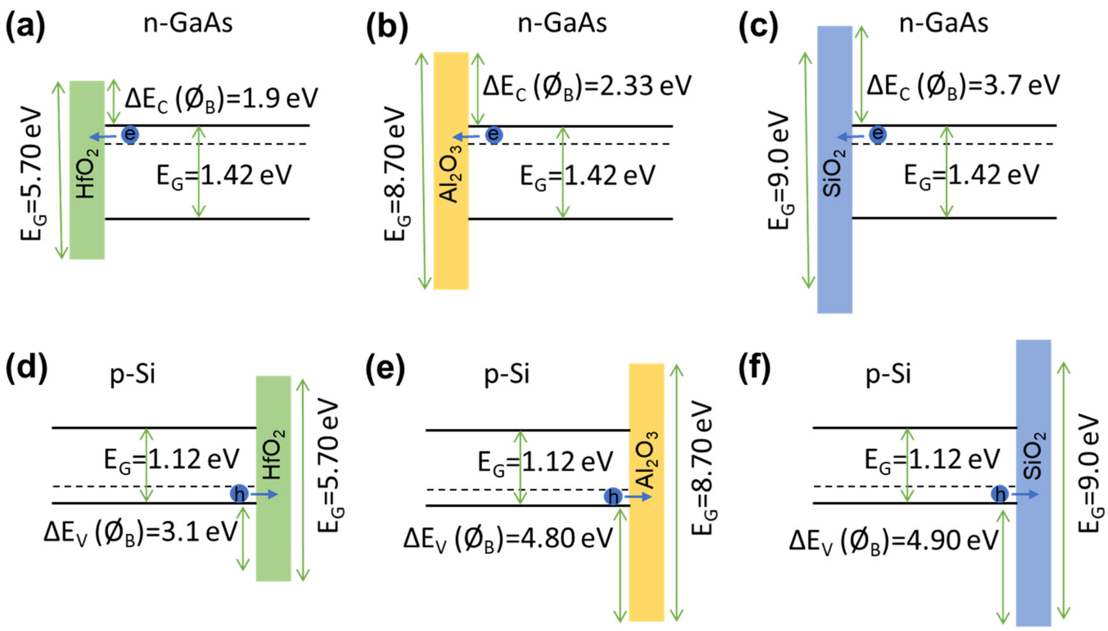

Figure S1. A schematic illustration of energy bandgap with (**a**–**c**) UO interfacial layers with n-GaAS and (**d**–**f**) UO interfacial layers with p-Si.

A COMSOL™ Multiphysics simulation was carried out to calculate the strain for different oxides and 2D materials induced at the heterointerface between p-Si and n-GaAs. A temperature-dependent strain calculation for different oxides (Al_2O_3, HfO_2, SiO_2) and 2D materials (graphene, h-BN) have been shown in Figure S2.

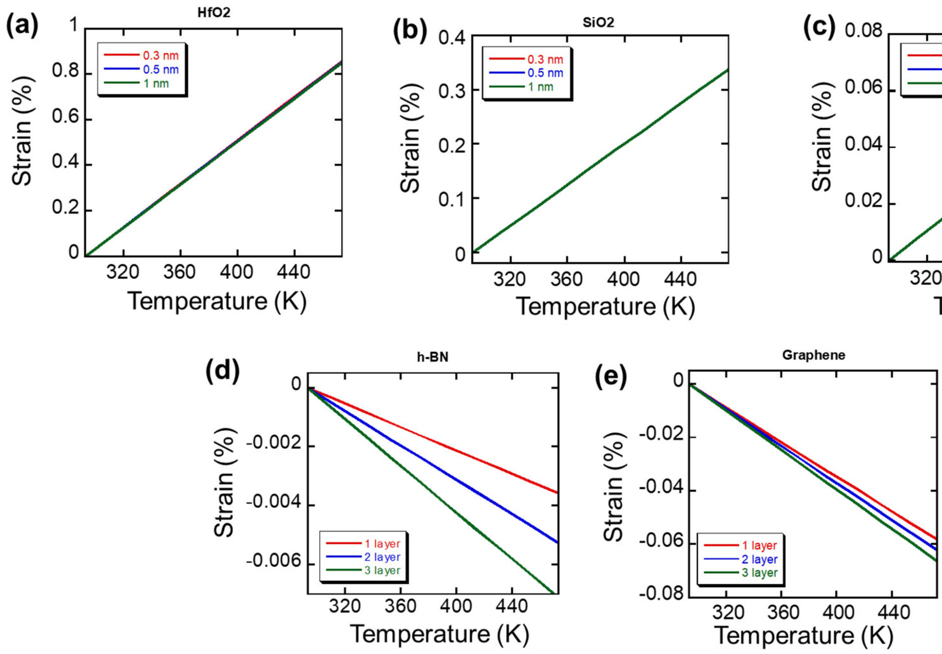

Figure S2. Simulated strain values of (**a**–**c**) UO interfacial layers and (**d**,**e**) 2D materials with different thicknesses as a function of temperature.

Table S1. The parameters for oxides (HfO_2, Al_2O_3, and SiO_2) and 2D materials (h-BN and graphene) that are used to calculate the transport property of the heterojunctions [1–27].

	HfO_2	Al_2O_3	SiO_2	h-BN	Graphene
Electron Effective mass (me*)	0.13 mo [1]	0.32 mo [2]	0.5 mo [3]	0.26 mo [4,5]	Monolayer: 0.012 mo [6] Bilayer: 0.041 mo [7] Trilayer: 0.052 mo[8]
Hole Effective mass (mh*)	0.58mo [9]	0.36mo [10]	0.33mo [11]	0.47 mo [12,13]	Monolayer: 0.013 mo Bilayer: 0.036 mo [14] Trilayer: 0.038 mo[15]
Band Gap (eV)	5.70 [1]	8.70 [1]	9.0 [1]	5.97 [17]	Close to 0, no more than 0.3 [16]
p-Si: Conduction band offset/barrier (eV)	1.5 [1]	2.8 [1]	3.1 [1]	1.0, 1.5 [17]	Monolayer: −0.74 eV Bilayer: −0.45 eV Trilayer: −0.46 eV
p-Si: Valence band offset/barrier (eV)	3.1	4.80	4.90	4.97, 4.47	Monolayer: 0.74 eV Bilayer: 0.45 eV Trilayer: 0.46 eV
n-GaAs: Conduction band offset/barrier (eV)	1.9	2.33 [18]	3.7 [19]	1.02 [20]	Monolayer: −0.68 eV [21] Bilayer: −0.75 eV [21] Trilayer: −0.78 [22]
n-GaAs: Valence band offset (eV)	2.38	4.95	3.88	4.95	Monolayer: 0.68 eV Bilayer: 0.75 eV Trilayer: 0.78 eV
Density (g/cm^{-3})	9.68	3.98	2.65	2.1	2.267
Thermal expansion coefficient (/K)	6 [23]	4.4×10^{-6} [24]	0.56 [25]	7.2 [26]	−3.75 [27]

Reference

1. Yijie, Z. and White, M.H. Modeling of direct tunneling current through interfacial oxide and high-K gate stacks. *Solid-State Electron*. **2004**, *48*, 1801–1807.
2. Huang, M.L.; Chang, Y.C.; Chang, C.H.; Lin, T.D.; Kwo, J.; Wu, T.B. and Hong, M. Energy-band parameters of atomic-layer-deposition Al2O3/InGaAs heterostructure. *Appl. Phys. Lett*. **2006**, *89*, 012903.
3. Brar, B.; Wilk, G.D. and Seabaugh, A.C. Direct extraction of the electron tunneling effective mass in ultrathin SiO2 *Appl. Phys. Lett*. **1996**, *69*, 2728.
4. Xu, Y.-N. and Ching, W.Y. Calculation of ground-state and optical properties of boron nitrides in the hexagonal, cubic, and wurtzite structures *Phys. Rev*. **1991**, *44*, 7787.
5. Barnett, B.L Ionizing and Non-ionizing Radiation Effects in Thin Layer Hexagonal Boron Nitride, M.S. thesis, Air Force Institute of Technology, USA, (2015).
6. Wang, G. Density functional study on the increment of carrier mobility in armchair graphene nanoribbons induced by Stone–Wales defects *Phys. Chem. Chem. Phys***.**, 2011,**13**, 11939–11945.
7. Zou, K.; Hong, X., and Zhu, J. Effective mass of electrons and holes in bilayer graphene: Electron-hole asymmetry and electron-electron interaction *Phys. Rev*. **2011**, *84*, 085408.
8. Zhang, Y.B.; Small, J.P.; Amori, M.E.S. and Kim, P. Electric field modulation of galvanomagnetic properties of mesoscopic graphite *Phys. Rev. Lett*. **2005**, *94*, 176803.
9. Bersch, E.; Rangan, S.; Bartynski, R.A.; Garfunkel, E. and Vescovo, E. Band offsets of ultrathin high- oxide films with Si *Phys. Rev*. **2008**, *78*, 085114.
10. Perevalov, T.V.; Shaposhnikov, A.V. and Gritsenko, V.A. Electronic structure of α-Al2O3: Ab initio simulations and comparison with experiment. *Jetp Lett*. **2007**, *85*, 165–168.
11. Vexler, M.I.; Tyaginov, S. and Shulekin, A.F. Determination of the hole effective mass in thin silicon dioxide film by means of an analysis of characteristics of a MOS tunnel emitter transistor. *J. Phys.: Condens. Matter*, **2005**, *17*, 8057-8068.
12. Bilal, M.; Xu, W.; Wang, C.; Wen, H.; Zhao, X.; Song, D.; Ding, L. Optoelectronic Properties of Monolayer Hexagonal Boron Nitride on Different Substrates Measured by Terahertz Time-Domain Spectroscopy. *Nanomater*. **2020**, *10*, 762.
13. Arnaud, B.; Lebègue, S.; Rabiller, P. and Alouani, M. Huge excitonic effects in layered hexagonal boron nitride. *Phys. Rev. Lett*. **2006**, *96*, 026402.
14. Avetisyan, A.A.; Partoens, B. and Peeters, F.M. Stacking order dependent electric field tuning of the band gap in graphene multilayers. *Phys. Rev.*, **2010**, *81*, 115432.
15. Kim, H.-Y.; Lee, K.; McEvoy, N.; Yim, C. and Duesberg, G.S. Chemically modulated graphene diodes *Nano Lett*, **2013**, *13*, 2182.
16. Chen, C.C.; Aykol, M.; Chang, C.-C.; Levi, A.F.J. and Cronin, S.B. Graphene-silicon Schottky diodes *Nano Lett*.,**2011** *11*, 1863.
17. Afanas'ev, V.V.; Chou, H.-Y.; Houssa, M.; Stesmans, A.; Lamagna, L.; Lamperti, A.; Molle, A.; Vincent, B., and Brammertz, G., Transitivity of band offsets between semiconductor heterojunctions and oxide insulators *Appl. Phys. Lett*.,**2011** *99*, 172101.
18. Hudait, M. K.; Zhu, Y.; Maurya, D.; Priya, S.; Patra, P.K.; Ma, A.W.K.; Aphale, A. and Macwan, I. Structural and band alignment properties of Al2O3 on epitaxial Ge grown on (100), (110), and (111)A GaAs substrates by molecular beam epitaxy. *J. Appl. Phys.*, **2013**, *113*, 134311.
19. Yang, J.-K.; Kim, W.S. and Park, H.-H. Chemical bonding states and energy band gap of SiO2-incorporated La2O3 films on n-GaAs (001). *Thin Solid Film*., **2006**, *494*, 311.
20. Li, X.; Lin, S.; Lin, X.; Xu, Z.; Wang, P.; Zhang, S.; Zhong, H.; Xu, W.; Wu, Z. and Fang, W. Graphene/h-BN/GaAs sandwich diode as solar cell and photodetector. *Opt. Express*, **2006**, *24*, 134.
21. Jie, W.; Zheng, F. and Hao, J. Graphene/gallium arsenide-based Schottky junction solar cells *Appl. Phys. Lett*., **2013**, *103*, 233111.
22. Tongay, S.; Schumann, T. and Hebard, A.F. Graphite based Schottky diodes formed on Si, GaAs, and 4H-SiC substrates. *Appl. Phys. Lett*., **2009**, *95*, 222103.
23. Haggerty, R.P.; Sarin, P.; Apostolov, Z.D.; Driemeyer, P.E. and Kriven, W.M. Thermal Expansion of HfO2 and ZrO2 Journal of the. *Am. Ceram. Soc*., **2014**, *97*, 2213.
24. Sah, R. E.; Driad, R.; Bernhardt, F.; Kirste, L.; Leancu, C.-C.; Czap, H.; Benkhelifa, F.; Mikulla, M. and Ambacher, O. Mechanical and electrical properties of plasma and thermal atomic layer deposited Al_2O_3 films on GaAs and Si, *J. Vac. Sci. Technol*., **2013** *31*, 041502.
25. Filipovic, L.: Topography Simulation of Novel Processing Techniques, Ph.D. thesis, TU Wien-Institute for Microelectronics, Austria (2012).
26. Singh, S.K.; Neek-Amal, M.; Costamagna, S. and Peeters, F.M. Thermomechanical properties of a single hexagonal boron nitride sheet. *Phys. Rev*.,**2013**, *87*, 184106.
27. Shaina, P.R.; George, L.; Yadav, V. and Jaiswal, M Estimating the thermal expansion coefficient of graphene: The role of graphene–substrate interactions. J. Phys.: Condens. Matter, **2016**, *28*, 085301.